Supporting Information

Ga-induced electronic structure engineering of $NiFe_2O_4$ nanosheet arrays for stable and efficient oxygen evolution

Sijie Chen [a], Haijun Liao [a], Xiaocheng Xu [a], Rui Wang [a], Zhipeng Sun [*, a], Le Huang [*, a]

[a]*School of Materials and Energy, Guangdong University of Technology, No. 100 Waihuan Xi Road, Guang zhou Higher Education Mega Center, Panyu District, Guangzhou 510006, P. R China.*

**Corresponding author [a.]:*

E-mail: zpsunxj@gdut.edu.cn (Zhipeng Sun); huangle@gdut.edu.cn (Le Huang).

Computational Method We utilize the Vienna *Ab* initio Simulation Package (VASP) [1] with the projector augmented-wave (PAW)[2] method to calculate the absorptive properties and electronic structures of $NiFe_2O_4$ and Ga-$NiFe_2O_4$. The energy convergence and force tolerance are set as 10^{-6} eV and 0.03 eV/Å, respectively. After optimization, the surface (100) was separated from the model and its catalytic performance was investigated. The exchange correlation adopts Perdew, Burke, and Ernzerhof (PBE) functional under the generalized gradient approximation (GGA) approach[3]. Moreover, the Hubbard *U* calibrations are implemented, the values of *U* are 4.5 eV[4] and 6.0 eV[5], respectively. To make sure the accuracy of calculations, Monkhorst-Pack k-grid employs k-mesh of 3×3×1 and 5×5×1 for structural relaxation and DOS calculation, respectively. The cutoff energy of plane-wave basis is set as 500 eV, and a vacuum layer is more than 15 Å to prevent interference from periodic images. The formation energy of defect (Ef defect) and doping (Ef doping) are defined by:

$$E_{defect}^{f} = E_{def-sys} + \mu_{Ni/Fe} - E_{pristine}$$

$E_{doping}^{f} = E_{doped-sys} - (E_{def-sys} + \mu_{Ga})$

where $E_{def-sys}$, $E_{pristine}$, $E_{doped-sys}$, $\mu_{Ni/Fe}$, and μ_{Ga} are the total energy of a defected system, pristine $NiFe_2O_4$, doped system, and chemical potential of Ni or Fe and Ga, respectively. The chemical potential of Ni, Fe, and Ga was obtained from the total energy of the bulk structure divided by the number of atoms.

The overall reaction and the four-electron reaction pathway of OER in alkaline media were considered as:

Overall reaction:

$4OH^- \rightarrow O_2 + 2H_2O + 4e^-$

$* + OH^- \rightarrow OH^* + e$

$OH^* + OH^- \rightarrow O^* + H_2O + e^-$

$O^* + OH^- \rightarrow OOH^* + e^-$

$OOH^* + OH^- \rightarrow * + O_2 + H_2O + e^-$

where * denotes the catalyst's active site. By employing H_2O and H_2 in the gas phase as a reference condition, the energy of adsorbates was estimated. The following equations were used to get the adsorption energies (△E) of each intermediate:

$\triangle E(OH^*) = E(OH^*) - E(^*) - (E(H_2O) - 0.5E(H_2))$

$\triangle E(O^*) = E(O^*) - E(^*) - (E(H_20) - E(H_2)$

$\triangle E(OOH^*) = E(OOH^*) - E(^*) - (2E(H_2O) - 1.5E(H_2))$

Each elementary reaction step's Gibbs free energy shift was identified as:

$\triangle G = \triangle E + \triangle ZPE - T\triangle S + \triangle GpH + \triangle GU$

the difference in zero-point energy and entropy between the adsorbed and free states at 298.15 K was denoted by ΔZPE and TΔS. ΔGpH = -kTln10·pH was used to calculate the influence of pH, and pH was adjusted to 14 to replicate alkaline conditions. A further definition for the contribution of the applied electrode potential was given as ΔGU= - n e U, where n, e, and U stand for the quantity of transferred electrons, elementary charge, and applied electrode potential, respectively. Following is how the limiting potential was determined:

$U_{onset} = \max\{\Delta G_1, \Delta G_2, \Delta G_3, \Delta G_4\}/e$

Where ΔG_1, ΔG_2, ΔG_3 and ΔG_4 were the free energy of each elementary steps. Equation was used to compute the overpotential:

$\eta = Uonset - 1.23(V)$

The energy band center of metal was expressed by equation:

$$\varepsilon = \frac{\int_{-\infty}^{+\infty} E \times \rho dE}{\int_{+\infty}^{-\infty} \rho dE}$$

Where the density of the metal atom's projected d state is denoted by the symbol ρ.

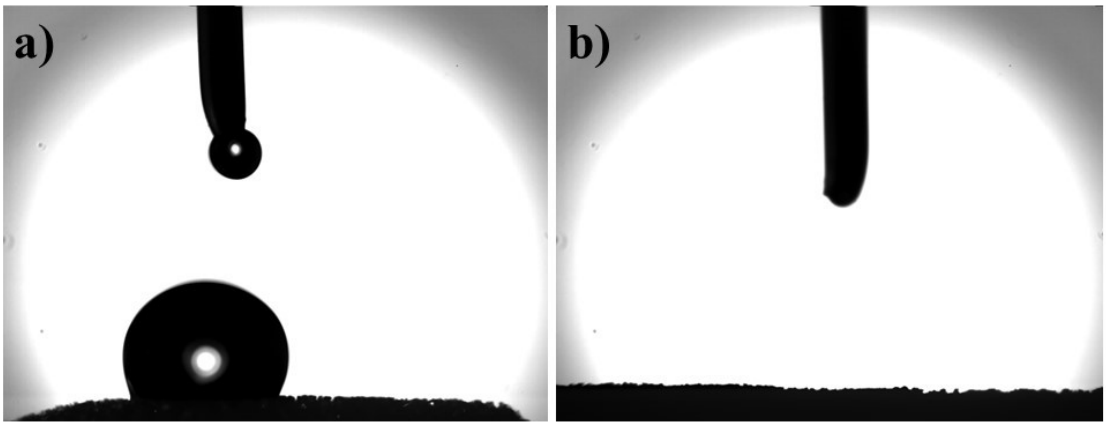

Fig. S1 Surface wettability of the (a) Ga-$NiFe_2O_4$, (b) NF.

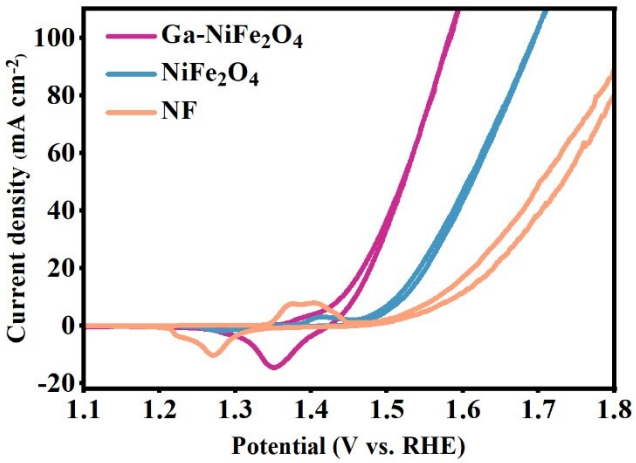

Fig S2 CV curves at a scan rate of 1 mV s^{-1} (without iR compensation)

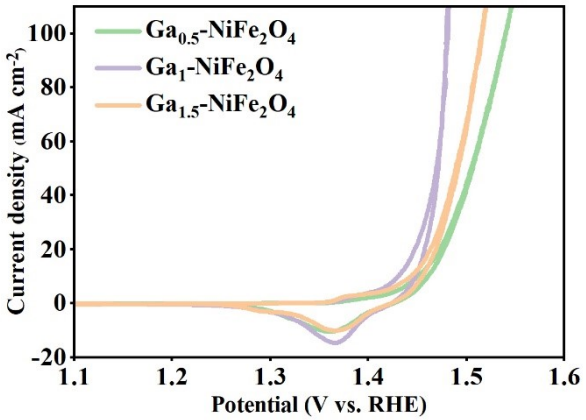

Fig. S3 CV curves of as-synthesized Ga-$NiFe_2O_4$ catalysts with different $Ga(NO_3)_3 \cdot xH_2O$ concentrations: 0.5 mmol $Ga(NO_3)_3 \cdot xH_2O$, 1 mmol $Ga(NO_3)_3 \cdot xH_2O$, and 1.5 mmol $Ga(NO_3)_3 \cdot xH_2O$.

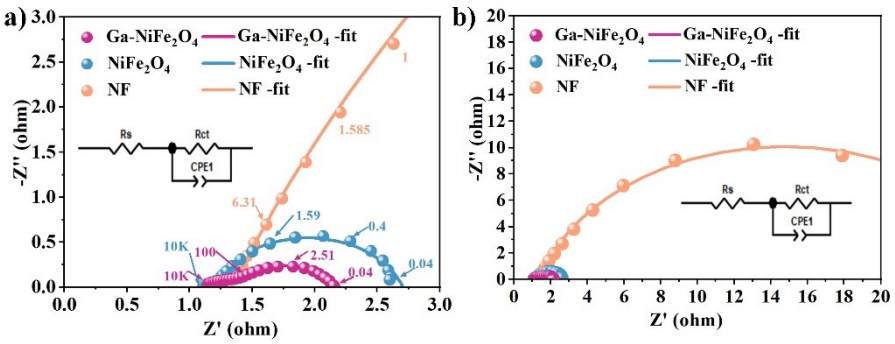

Fig. S4 (a) Nyquist plots with some frequencies, (b) The complete Nyquist plots

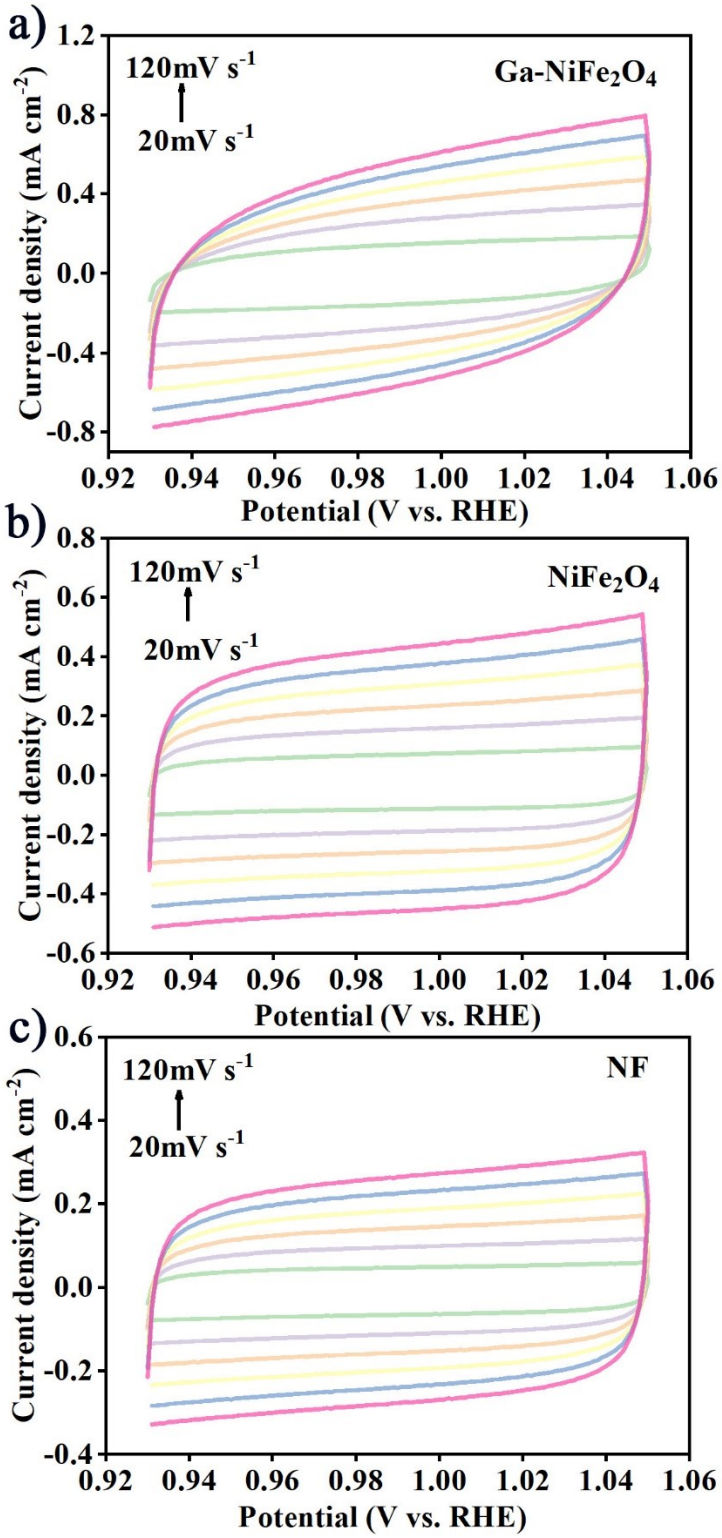

Fig. S5 CV curves of (a) Ga-$NiFe_2O_4$, (b) $NiFe_2O_4$, and (c) NF obtained in a potential window of 0.93 to 1.03V versus RHE at different scan rates.

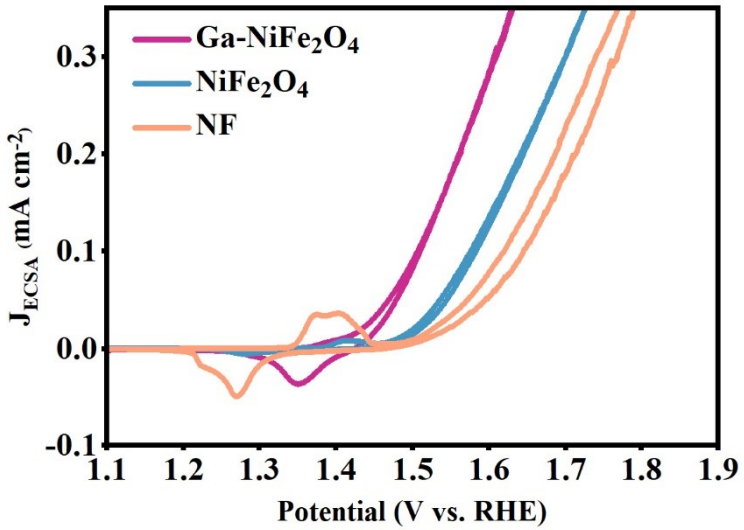

Fig. S6 ECSA-normalized OER activity (scan rate: 1 mV s^{-1})

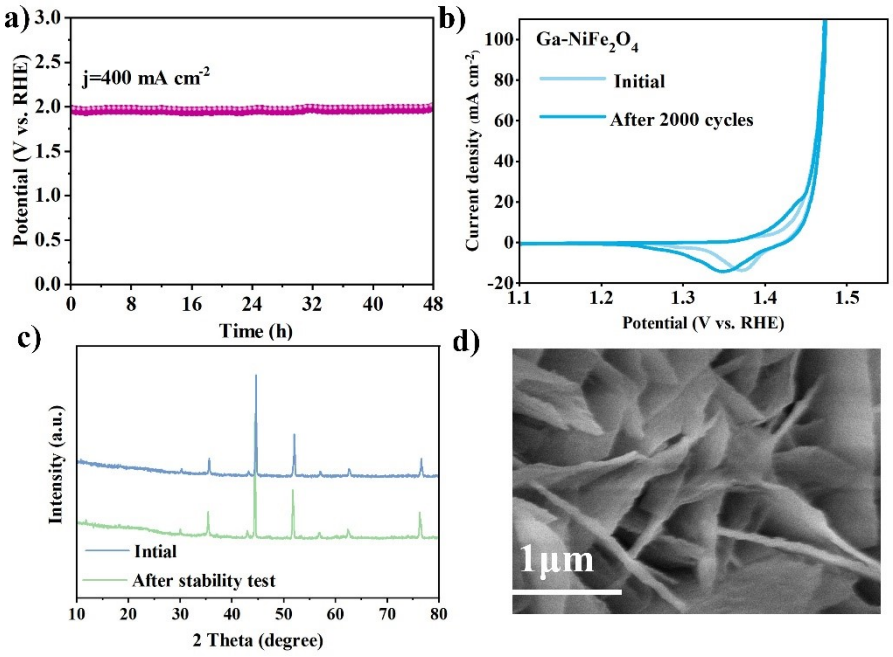

Fig. S7 (a) Chronopotentiometry curves of the Ga-$NiFe_2O_4$ in 1 M KOH at a current density of 400 mA cm^{-2}, (b) CV curves before and after 2,000 cycles CV sweeps of Ga-$NiFe_2O_4$ (scan rate: 1 mV s^{-1}), (c) XRD image and (d) SEM of Ga-$NiFe_2O_4$ after OER stability testing.

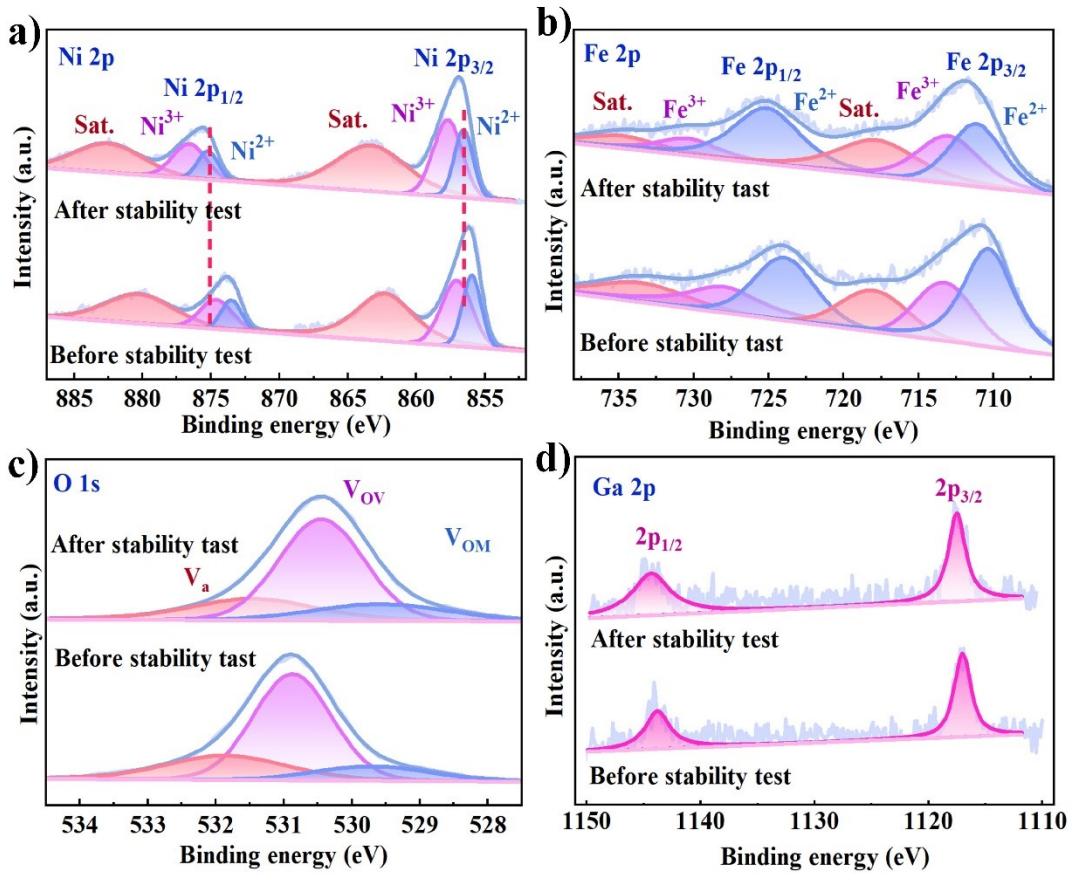

Fig. S8 (a) Ni 2p, (b) Fe 2p, (c) O 1s and (d) Ga 2p XPS spectra of Ga-$NiFe_2O_4$ before and after OER stability testing in 1 M KOH.

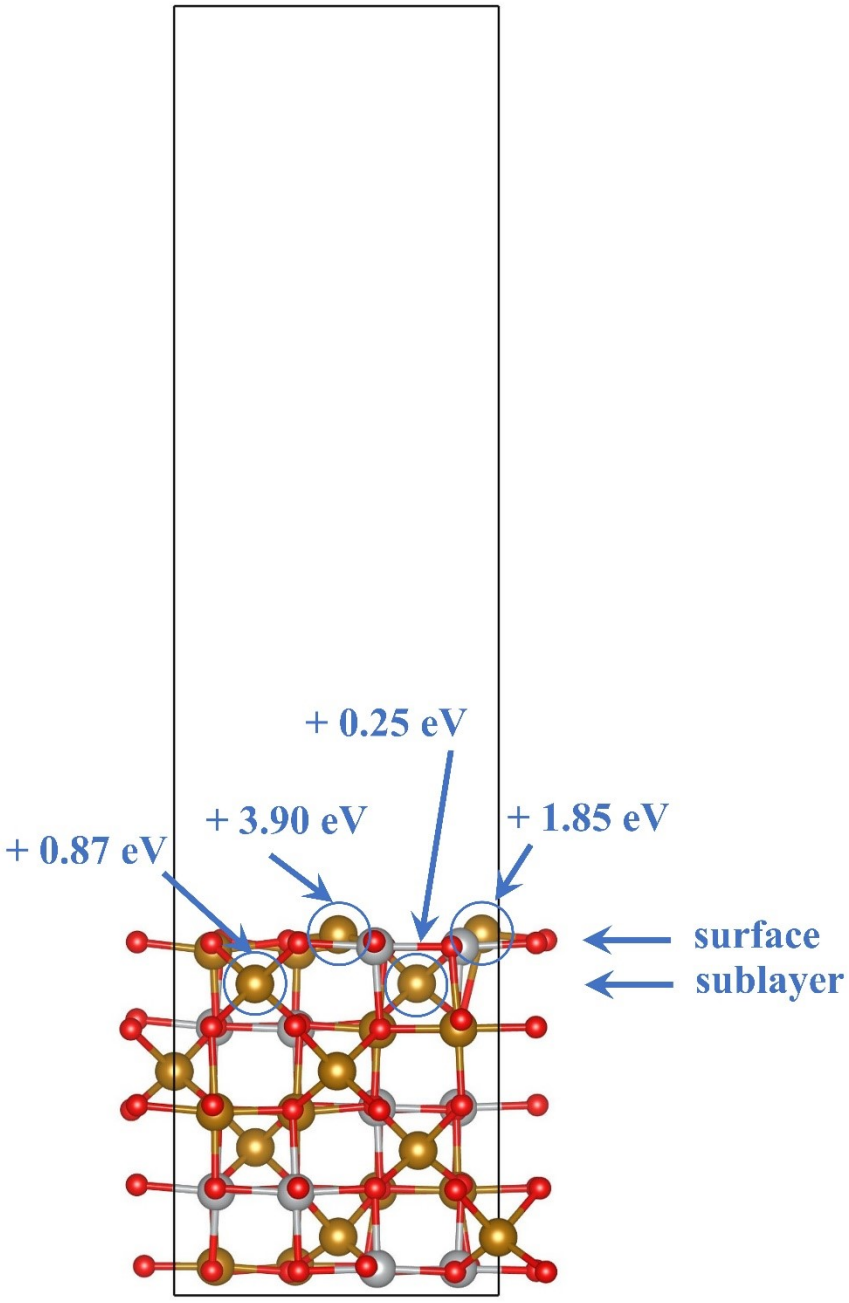

Fig. S9 The calculated Ga doping energy at each site on the Fe tetrahedron is specified at the end of the arrow.

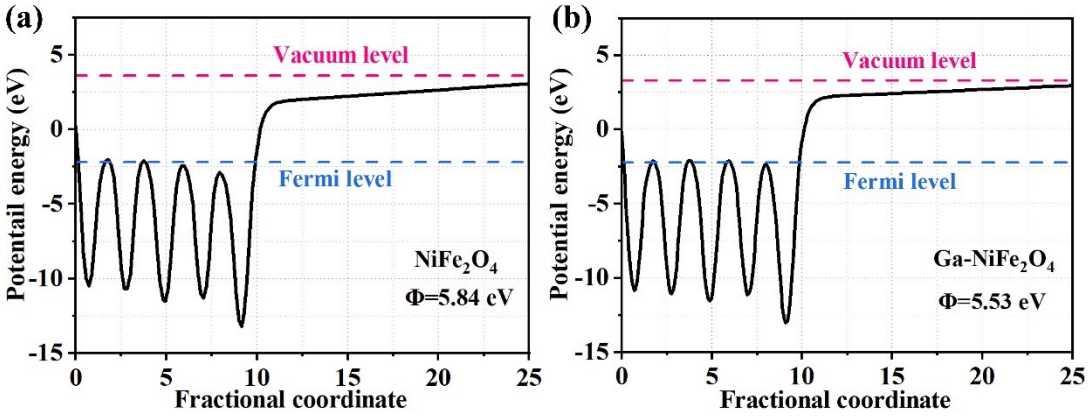

Fig. S10 Schematic diagram of the work function

Table S1 The values of R_s and R_{ct} for catalyst

	Ga-$NiFe_2O_4$	**$NiFe_2O_4$**	**NF**
R_s (Ω)	1.27	1.26	1.37
R_{ct} (Ω)	2.18	5.03	26.05

Table S2 Comparison of the OER performance of various catalysts

Catalyst	***J*** **(mA cm^{-2})**	***η*** **(mV)**	**Ref.**
Ga-$NiFe_2O_4$	*10*	218	This work
NiFe LDH@SnO_2/NF	10	234	6
F-Ni_3S_2	10	239	7
FNMCO-6/NF	10	240	8
Fe,Ni-CoS_2	10	242	9
Ce/N-NiO	10	250	10
$NiFe_2O_4$@FNF	10	262	11
$Co(OH)F/Ni(OH)_2$@$Fe(OH)_3$	10	270	12
$NiCo_2S_4$@NiFe LDH	10	287	13

Table S3 Comparison of the overall water splitting performance of various catalysts

Catalyst	***J*** **(mA cm^{-2})**	***η*** **(mV)**	**Ref.**
Ga-$NiFe_2O_4$	10	1.59	This work
NiFe-LDH/$Ni(OH)_2$	10	1.6	14
Ni_3S_2@Ni_2P/MoS_2	10	1.61	[1]5
Ni–Fe_2B	10	1.64	16
NiFe LDH@CoP/NiP_3	10	1.64	17
Fe_3O_4/NiFe LDH/Fe_3O_4	10	1.648	18
NiFe-LDH@Ni_3S_2	10	1.65	19
$CoCO_3$@NiFe LDH	10	1.67	20
NiFe-LDH/$FeCoS_2$/CFC	10	1.74	21

Table S4 Calculated d-band center of each active site for $NiFe_2O_4$ and Ga-$NiFe_2O_4$

	Fe_{Td}	Fe_{Oh}	Ni	Ga
$NiFe_2O_4$	-2.47 eV	-2.94 eV	-2.73 eV	
Ga-$NiFe_2O_4$	-2.07 eV	-2.59 eV	-2.57 eV	-12.77 eV

References:

1 G. Kresse and J. Furthmüller, Efficient Iterative Schemes for ab Initio Total-Energy Calculations Using a Plane-Wave Basis Set. *Phys. Rev. B*, 1996, **54**, 11169–11186.

2 J. J. Mortensen, L. B. Hansen and K. W. Jacobsen, Real-Space Grid Implementation of the Projector Augmented Wave Method. *Phys. Rev. B*, 2005, **71**, 035109.

3 J. P. Perdew, K. Burke and M. Ernzerhof, Generalized Gradient Approximation Made Simple. *Phys. Rev. Lett.*, 1996, **77**, 3865–3868.

4 H. A. Babu and H. Wanare, Negative and Positive Hysteresis in Double-Cavity Optical Bistability in a Three-Level Atom. *Phys. Rev. A*, 2011, **83**, 033818.

5 A. Jain, G. Hautier, C. J. Moore, S. Ping Ong, C. C. Fischer, T. Mueller, K. A. Persson and G. Ceder, A High-Throughput Infrastructure for Density Functional Theory Calculations. *Comput. Mater. Sci.*, 2011, **50**, 2295–2310.

6 C. Wan, J. Jin, X. Wei, S. Chen, Y. Zhang, T. Zhu and H. Qu, Inducing the SnO_2-Based Electron Transport Layer into NiFe LDH/NF as Efficient Catalyst for OER and Methanol Oxidation Reaction. *Journal of Materials Science & Technology*, 2022, **124**, 102–108.

7 Q. Xu, M. Chu, M. Liu, J. Zhang, H. Jiang and C. Li, Fluorine-triggered Surface Reconstruction of Ni_3S_2 Electrocatalysts towards Enhanced Water Oxidation. *Chem. Eng. J.*, 2021, **411**, 128488.

8 H. Shi, Q. Zha and Y. Ni, Fe-doped (Ni,Mn)Co_2O_4 Nanorod Arrays on Ni Foam as Highly Efficient Electrocatalyst for Oxygen Evolution Reaction in Alkaline and Neutral Conditions with Superb Long-Term Stability. *J. Alloys Compd.*, 2022, **904**, 164052.

9 W. Peng, A. Deshmukh, N. Chen, Z. Lv, S. Zhao, J. Li, B. Yan, X. Gao, L. Shang, Y. Gong, L. Wu, M. Chen, T. Zhang and H. Gou, Deciphering the Dynamic Structure Evolution of Fe and Ni-Co Doped CoS_2 for Enhanced Water Oxidation. *ACS Catal.*, 2022, **12**, 3743–3751.

10 F. Yang, X. Zhang, L. Zhou, S. Lin, X. Cao, J. Jiang and X. Lu, Tuning the interfacial electronic coupling of NiO via CeO_2 and nitrogen Co-decoration for highly efficient oxygen evolution reaction. *Chem. Eng. J.*, 2022, **432**, 134255.

11 J. Liu, H. Yuan, Z. Wang, J. Li, M. Yang, L. Cao, G. Liu, D. Qian and Z. Lu, Self-Supported Nickel Iron Oxide Nanospindles with High Hydrophilicity for Efficient Oxygen Evolution. *Chem. Commun.*, 2019, **55**, 10860–10863.

12 H. Jiu, H. Wei, C. Wang, S. Che, Z. Guo, Y. Han, Q. Xu, X. Yu and L. Zhang, Construction of Co(OH)F/$Ni(OH)_2$@$Fe(OH)_3$ Core-Shell Heterojunction on Nickel Foam for Efficient Oxygen Evolution. *Int. J. Hydrog. Energy*, 2022, **47**, 33719–33727.

13 X. Feng, Q. Jiao, W. Chen, Y. Dang, Z. Dai, S. L. Suib, J. Zhang, Y. Zhao, H. Li and C. Feng, Cactus-like $NiCo_2S_4$@NiFe LDH Hollow Spheres as an Effective Oxygen Bifunctional Electrocatalyst in Alkaline Solution. *Appl. Catal. B*, 2021, **286**, 119869.

14 N. S. Gultom, H. Abdullah, C.-N. Hsu and D.-H. Kuo, Activating Nickel Iron Layer Double Hydroxide for Alkaline Hydrogen Evolution Reaction and Overall Water Splitting by Electrodepositing Nickel Hydroxide. *Chem. Eng. J.*, 2021, **419**, 129608.

15 X. Yu, S. Xu, Z. Wang, S. Wang, J. Zhang, Q. Liu, Y. Luo, Y. Du, X. Sun and Q. Wu, Self-Supported Ni_3S_2@Ni_2P/MoS_2 Heterostructures on Nickel Foam for an Outstanding Oxygen Evolution Reaction and Efficient Overall Water Splitting. *Dalton Trans.*, 2021, **50**, 15094–15102.

16 R. Yao, Y. Wu, Q. Zhao, J. Li and G. Liu, Autogenous Growth of Highly Active Bifunctional Ni–Fe_2B Nanosheet Arrays toward Efficient Overall Water Splitting. *Int. J. Hydrog. Energy*, 2022, **47**, 8303–8313.

17 C. Song, Y. Liu, Y. Wang, S. Tang, W. Li, Q. Li, J. Zeng, L. Chen, H. Peng and Y. Lei, Highly Efficient Oxygen Evolution and Stable Water Splitting by Coupling NiFe LDH with Metal Phosphides. *Sci. China Mater.*, 2021, **64**, 1662–1670.

18 X. Zhang, Y. Qiu, Q. Li, F. Liu, L. Cui, C. Li and J. Liu, Sandwich Structured Fe_3O_4/NiFe LDH/Fe_3O_4 as a Bifunctional Electrocatalyst with Superior Stability for Highly Sustained Overall Water Splitting. *J. Alloys Compd.*, 2023, **932**, 167612.

19 L. Ren, C. Wang, W. Li, R. Dong, H. Sun, N. Liu and B. Geng, Heterostructural NiFe-LDH@Ni_3S_2 Nanosheet Arrays as an Efficient Electrocatalyst for Overall Water Splitting. *Electrochim. Acta*, 2019, **318**, 42–50.

20 R. Que, S. Liu, P. He, Y. Yang and Y. Pan, Hierarchical Heterostructure $CoCO_3$@NiFe LDH Nanowires Array as Outstanding Bifunctional Electrocatalysts for Overall Water Splitting. *Mater. Lett.*, 2020, **277**, 128285.

21 Z. Zhang, J. Zhou, H. Wei, Y. Dai, S. Li, H. Shi and G. Xu, Construction of Hierarchical NiFe-LDH/$FeCoS_2$/CFC Composites as Efficient Bifunctional Electrocatalysts for Hydrogen and Oxygen Evolution Reaction. *J Mater Sci*, 2020, **55**, 16625–16640.